THE JOURNAL OF PHYSICAL CHEMISTRY A

Article

pubs.acs.org/JPCA

Imaging the Photodissociation Dynamics of Nitrous Acid (HONO): The Role of Torsion

Published as part of The Journal of Physical Chemistry virtual special issue "Veronica Vaida Festschrift".

Chandika Amarasinghe, Alexander Kamasah, Casey D. Foley, James O. F. Thompson, and Arthur G. Suits*

Department of Chemistry, University of Missouri, Columbia, Missouri 65211, United States

ABSTRACT: We present the findings of the first imaging study of *trans*-HONO and *cis*-HONO photodissociation through the 2_0^2 band and 2_0^1 band of the $\tilde{A}^1A''-\tilde{X}^1A'$ transition. The NO photofragment was probed by (1 + 1) resonance-enhanced multiphoton ionization and studied using the direct-current slice imaging technique with our finite slice reconstruction method. The NO state-specific translational energy distributions show some rotational structure corresponding to the internal state distribution in the OH cofragment. All images showed a perpendicular angular distribution with a recoil anisotropy parameter from ca. −0.6 to −0.8. In both bands, *cis*-HONO showed greater anisotropy than *trans*-HONO. Deviation from the limiting value expected for a pure perpendicular dissociation is ascribed to deviation of the transition moment from normal to the heavy atom plane owing to OH torsion, rather than lifetime effects assumed in the large body of previous work.

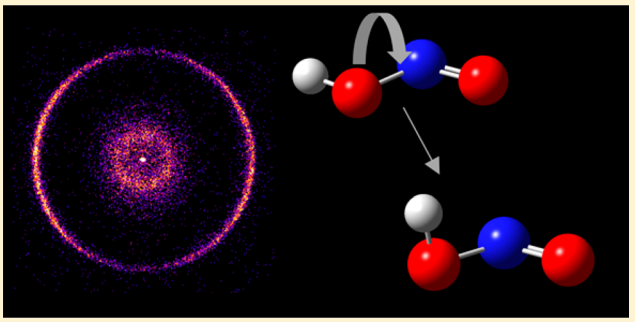

INTRODUCTION

The hydroxyl radical (OH) is arguably the most important radical in the atmosphere. It is the main atmospheric oxidant, responsible for removal of most of the gas pollutants in the troposphere.[1,2] As a major source of OH, nitrous acid (HONO) is one of the key molecules present in the atmosphere.[3−7] A study in the summer in New York found that 56% of the OH produced in the daytime was produced by photodissociation of HONO.[8] HONO was also found to be the major source of OH at dawn.[1] Motivated by these considerations, photodissociation of HONO has been studied extensively by both theoretical and experimental chemists. It is also a relatively simple system for which both diatomic products can be detected with quantum state specificity. This has also motivated detailed dynamical investigations, notably by Vasudev and co-workers.[9−15]

In 1962, G.W. King and D. Moule presented the UV absorption spectrum of HONO and showed that lowest energy transition $\tilde{A}^1A''-\tilde{X}^1A'$ of HONO occurs between 300 and 400 nm, dominated by the progression $2_0^{v'}$ in the ν_2 vibrational mode.[16] Much later, Vasudev and co-workers noted that the earlier assignment was uncertain by one quanta of ν_2' for *cis*-HONO due to spectral congestion.[12] They assigned the weak transitions that were red-shifted from the *trans*-HONO $2_0^{v'}$ transitions to *cis*-HONO $2_0^{v'}5_0^1$ combination bands. Later Schurath and co-workers[17] assigned those transitions to *trans*-HONO $2_0^{v'}4_0^1$ combination bands; their absorption spectrum is given in Figure 1 to aid the following discussion. The ν_2 mode

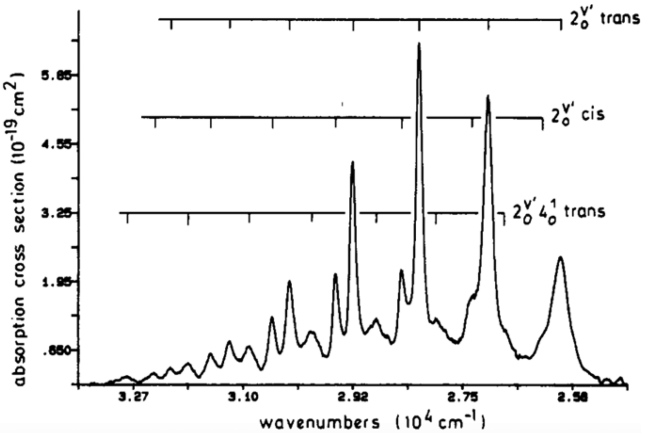

Figure 1. Absorption spectrum of HONO by Schurath and co-workers showing the progressions of *trans* and *cis*-HONO. Reprinted with permission from A. Bongartz, J. Kames, F. Welter, and U. Schurath, *J. Phys. Chem.*, 1991, 95, 1076−1082. Copyright 1991 American Chemical Society.

was attributed to the N═O stretch and the electronic transition assigned to the excitation of a nonbonding electron of the terminal oxygen to an antibonding π^* orbital of N═O.

Received: August 14, 2017
Revised: September 15, 2017
Published: September 20, 2017

DOI: 10.1021/acs.jpca.7b08120
J. Phys. Chem. A 2017, 121, 7503−7510

The $\tilde{A}^1A''$ excited state then dissociates to give OH and NO in ground $^2\Pi$ states:[18]

$$HONO(\tilde{X}^1A') + h\nu \rightarrow OH(\tilde{X}^2\Pi) + NO(\tilde{X}^2\Pi)$$
$$D_0 = 16\,772 \pm 14 cm^{-1}$$

The complete characterization of the OH fragment produced from the *trans*-HONO $\tilde{A}(S_1)$ state dissociation has been accomplished by Vasudev and Zare based on a Doppler spectroscopy study.[14,15] They found the product OH to be rotationally cold, and based on the absence of any hot bands, they concluded that the OH fragment is also vibrationally cold. They also found that the spin−orbit component F_2 of the OH photofragment was more highly populated than F_1. Furthermore, they concluded that the excited state has A'' symmetry and is planar. The transition moment is thus strictly perpendicular to the plane of the molecule at the equilibrium geometry. In 1989, Dixon and Rieley characterized the NO fragment produced by *trans*-HONO photodissociated via the 2_0^2 band using laser-induced fluorescence (LIF).[19] They inferred that the NO fragment is rotationally hot and vibrationally excited as well. They also found that the NO fragment had a positive rotational alignment. Further studies have reported the NO vibrational populations for all $2_0^{\nu'}$ bands.[9,10]

HONO consists of two conformational isomers, namely, *trans*-HONO and *cis*-HONO. Both experimental and computational studies have shown that *trans*-HONO is more stable at room temperature than *cis*-HONO.[17,20−23] The most recent studies show that the energy difference is as low as 124 cm^{-1}.[24−26] Finnigan and co-workers were the first to propose that there can be some intramolecular hydrogen bonding interaction in *cis*-HONO based on comparison of the force constants of the two conformers.[27] The smaller value for the OH force constant as well as the high positive value for the interaction between N−O stretch and NOH bend in *cis*-HONO suggests that there likely is some intramolecular hydrogen bonding between the terminal oxygen and the cis hydrogen. In fact, this observation is in agreement with computational studies that were done later for the system.[28,29] Vasudev and co-workers were the first to study the influence of this intramolecular hydrogen bonding on photodissociation dynamics and showed that the rotational temperatures and the orbital anisotropy of the ejected OH fragment increased with the increasing ν_2 content.[11]

In the present experiment, we study both *cis* and *trans*-HONO dissociation via the 2_0^2 band and 2_0^1 band of the $\tilde{A}^1A''-\tilde{X}^1A'$ transition and investigate their dissociation dynamics. The focus of this study is mainly on the photofragment angular and translational energy distribution of the two HONO conformers using ion imaging. We note that our present detection scheme is not sensitive to any alignment effects.

The ion imaging technique was first introduced in 1987 by Chandler and Houston,[30] which was then greatly improved after a decade with development of high-resolution velocity map imaging by Eppink and Parker.[31] Further development of velocity map imaging was achieved by the introduction of direct-current (DC) slice imaging in 2003.[32] DC slice imaging provides direct information about the angular distribution, translational energy release, and angular momentum polarization. Slice imaging can be further enhanced with the use of our recently developed Finite Slice Analysis algorithm (FinA) as shown below. In this article, we present the first imaging study of this system, allowing for more precise angular and translational energy distributions to be obtained than in earlier Doppler studies. A reexamination of the literature in light of our current results suggests a key role for coupling to torsion in the initial excitation, rather than lifetime effects, to account for deviation from limiting anisotropy in the angular distributions.

EXPERIMENTAL SECTION

A concise description of the apparatus that is relevant to the experiment is presented in this section, and the detailed DC slice imaging setup can be found elsewhere.[32] The apparatus consists of two chambers, the source chamber and detection chamber, pumped by two different turbomolecular pumps. The chambers were separated by an aluminum plate with the skimmer mounted to it. The skimmed and supersonically expanded molecular beam interacted with the laser beams in the region between the Repeller and the first Extractor lenses of the DC slice ion optics setup, which then accelerated the produced ions to a position-sensitive detector.

HONO was prepared by a method similar to that described by Dixon and Rieley, producing HONO with minimal contamination from NO_2.[19] $NaNO_2$ (10 mL of 1 M) was first degassed under vacuum, and then 5 mL of 1 M H_2SO_4 was added to the mixture. Helium gas then was bubbled through the mixture at a backing pressure of 1.3 bar. The gas mixture was introduced to the source chamber by a commercial solenoid pulsed valve operating at 10 Hz and 400 μs nominal pulse width. Polytetrafluoroethylene (PTFE) tubing was used where possible, and the length from the bubbler to the valve was kept at a minimum to reduce the surface catalysis that promotes reaction to equilibrium:

$$2HONO \leftrightarrow NO + NO_2 + H_2O$$

The molecular beam containing HONO and small impurities of NO and NO_2 in helium was skimmed and then crossed by the two counter propagating laser beams at right angles in the interaction region. The dissociation via the 2_0^2 band was performed using 354.40 nm light for *trans*-HONO and 351.30 nm light for *cis*-HONO. This light was generated by doubling the output of a pulsed dye laser (Sirah, pyridine 1/ethanol) pumped by the second harmonic of a Nd:YAG laser. Dissociation via the 2_0^1 band was achieved using 368.30 nm light for *trans*-HONO and 364.40 nm light for *cis*-HONO. This beam was generated by the same pulsed dye laser (Sirah, styryl 8/ethanol). The initial horizontally polarized pump laser beam was sent through a Berek's Compensator set at half wave retardation to make it vertical (parallel to the detector plane), and the polarization was carefully verified by a MgF_2 Rochon Prism. The beam was focused to the interaction region by a UV fused silica lens (f = 300 mm). The tunable probe laser beam was generated by frequency mixing of the third harmonic of a seeded Nd:YAG laser with the fundamental output of a pulsed dye laser (Sirah, mix Rh B/Rh 101 in ethanol) pumped by the second harmonic of the same Nd:YAG laser. The polarization of the probe laser was kept horizontal, and the beam was focused by a UV fused silica lens (f = 250 mm). The probe laser wavelength was adjusted according to the NO rotational levels assigned by LIFBASE software,[33] and all wavelengths were verified and monitored by a wavemeter (COHERENT Wavemaster). The power of the probe laser was kept at ∼0.5 mJ/pulse, and the dissociation laser was operated at ∼3 mJ/pulse. The temporal delay between the probe and the pump

DOI: 10.1021/acs.jpca.7b08120
J. Phys. Chem. A 2017, 121, 7503−7510

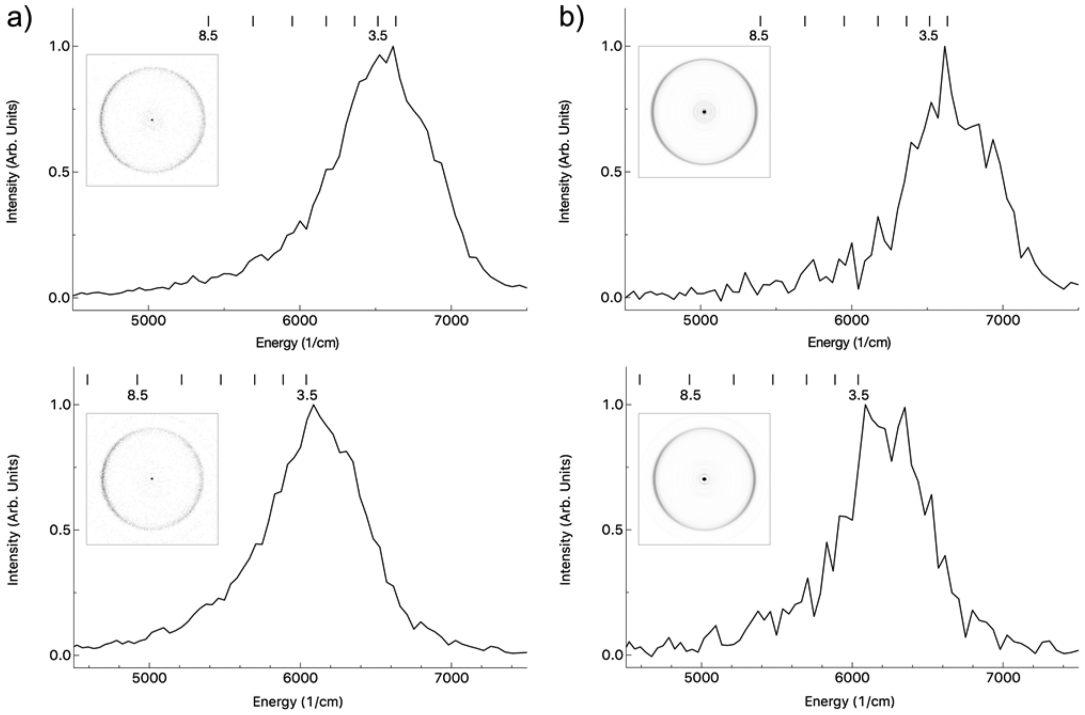

Figure 2. (a) Raw DC sliced image of NO (v = 2, J = 25.5 (upper panel), J = 30.5 (lower panel)) from photodissociation of *trans*-HONO via 2_0^2 band at 354.40 nm and the total translational energy distribution. (b) FinA reconstructions of the corresponding images. Combs reflect cofragment OH(v = 0) rotational distribution.

lasers was ∼10 ns. The ionization was effected by (1 + 1) resonance enhanced multi-photon ionization (REMPI), and the produced ions were focused to the detector by a DC slice ion optic setup.[32] The 75 mm diameter detector (BOS-75-OPT01, Beam Imaging Solutions) consists of two microchannel plates coupled to a P47 phosphor screen. The detector was gated (75 ns) to image only the central slice of the NO^+ fragment. The positions of the ions were captured by a CCD camera, and the acquisition was performed by our in-house NuAcq software. A photomultiplier tube was used to obtain timing information on the ions.

RESULTS

Photodissociation via the 2_0^2 band. The dissociation wavelengths for both conformers of HONO were chosen based on previously published absorption spectra.[17,34] The vibrational and rotational distributions of the NO photofragment produced by dissociation via the 2_0^2 band were previously characterized by Dixon and Riley.[19] They estimated the vibrational populations to be 2:1:0.01 for NO in v = 1, 2, and 3, respectively. They also found the rotational distributions for both v = 2 and v = 3 to range from 10.5 to 40.5, peaking at ∼25.5. In our experiments, we first probed v = 2 to reduce the interference arising from NO_2, since at this wavelength NO produced by NO_2 will also occupy v = 1. Probing was done via the Q_{11} + P_{21} transitions. The acquired raw images were reconstructed using the FinA program recently developed in our lab.[35,36] For comparison, the translational energy distributions from raw integration and the polar FinA Fit reconstructions used through this work are shown for one set of images in Figure 2. The effective slice width of the measurements was determined to be 25% at 370 pixels.

It can be seen in the spectra that reconstruction recovers the cofragment OH rotational distribution much better than the raw spectrum. It is also evident from the spectrum that the cofragment OH appears in rotationally excited levels up to $J \approx$ 8.5. To find the corresponding rotational temperature of the OH fragment, a simulation (Figure 3) was done by plotting

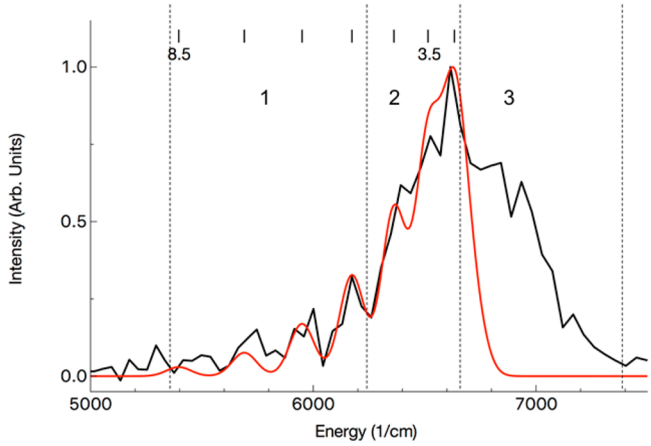

Figure 3. FinA reconstruction of the total translational energy distribution of NO (J'' = 25.5) from photodissociation of *trans*-HONO via 2_0^2 band at 354.40 nm (black) and the simulation assuming a rotational temperature of 398 K (red).

Gaussians for each cofragment F_1 spin−orbit level of OH and summing them. The blurring due to electron recoil upon ionization was taken as the full width at half-maximum (fwhm) for each Gaussian. The simulation assumes that the rotational distribution follows a Boltzmann distribution, which need not be the case. The simulation fits reasonably well with the slower side, but it does not reproduce the fast edge. To describe this

DOI: 10.1021/acs.jpca.7b08120
J. Phys. Chem. A 2017, 121, 7503−7510

Table 1. Rotational Temperatures of F1 Spin−Orbit Component of OH(v = 0) Cofragment and Corresponding Recoil Anisotropy Parameters for Regions 1, 2, and 3 Photodissociation via 2_0^1 and 2_0^2 Bands for Both Conformers

					anisotropy parameter (β)[b]		
dissociation band	conformer	NO vib level (v'')	NO rotational level (J'')	rotational temperature[a] (K) of OH	region 1	region 2	region 3
2_0^2	*trans*	2	25.5	398	−0.49	−0.66	−0.29
			30.5	385	−0.44	−0.71	−0.45
	cis		25.5	440	−0.53	−0.70	−0.47
2_0^1	*trans*	1	25.5	425	−0.81	−0.69	−0.53
			30.5	390	−0.57	−0.75	−0.49
	cis		25.5	440	−0.74	−0.83	−0.64
			30.5	400	−0.77	−0.80	−0.63

[a] ±10%. [b] ±0.05.

feature, we must consider the possibility of a hot band within our spectrum. This will be considered in the discussion section below.

These simulations of the NO J = 25.5 and 30.5 translational energy distributions following the 2_0^2 band photolysis yielded rotational temperatures of the OH cofragment of 398 and 385 K, respectively. The recoil anisotropy parameter (β) for the two images was measured by plotting the angular distribution and fitting it to the equation $I(\theta) \propto 1 + \beta P_2(\cos\theta)$, where I is the intensity, θ is the angle between the electric vector of the photodissociation laser, and the recoil direction of the photofragment and P_2 is the second-order Legendre polynomial. We separated the spectra into three regions depending on their energies (see Figure 3). Region one corresponds to high J (5.5−8.5) OH, Region 2 corresponds to low J (1.5−5.5) OH, and region 3 corresponds to the fast edge. The anisotropy parameters obtained for J = 25.5 for regions 1, 2, and 3 were −0.49, −0.66, and −0.29, respectively. For J = 30.5 the anisotropy parameters were found to be −0.44, −0.71, and −0.45 for these three regions. Rotational temperatures and anisotropy parameters for all transitions are compiled in Table 1. Looking at the trends, it is clear that going from OH low J to high J the anisotropy decreases and that the fast edge is more isotropic compared to the peak and to the slow edge.

cis-HONO was dissociated in the 2_0^2band at 351.30 nm, where it has its maximum absorption cross section. The resulting raw sliced image and corresponding translational energy distribution are shown in Figure 4 for NO J = 25.5. Compared to *trans*-HONO, the rotational temperature (440 K) of OH formed in conjunction with *cis*-HONO was slightly higher. The recoil anisotropy parameter for the three regions was found to be −0.53, −0.70, and −0.47. In region 2 (low J) the anisotropy slightly increased compared to *trans*-HONO (β = −0. 70 vs −0.66 for trans) but within the experimental uncertainties, although the same thing was observed for region 1 as well. However, the striking difference is in region 3, where β changed from −0.29 to −0.47. This effect will be examined in detail in the discussion section. The molecular beam consists of both *cis* and *trans*-HONO, and there could be some contribution from *trans* excitation here as well, although it is expected to be small. Therefore, the underlying anisotropy of pure *cis*-HONO could be somewhat higher than measured here.

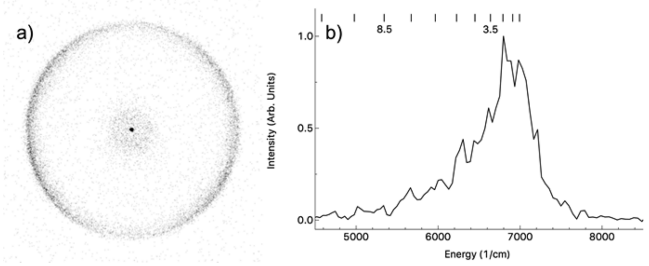

Figure 4. (a) Raw DC sliced image of NO (v'' = 2, J'' = 25.5) from photodissociation of *cis*-HONO via 2_0^2 band at 351.30 nm. (b) Corresponding FinA reconstructed total translational energy distribution.

Photodissociation via the 2_0^1 Band. *trans*-HONO was photodissociated at 368.30 nm, where it has the maximum absorption cross section for the 2_0^1 band. NO fragments resulting from this dissociation largely occupy v = 0 and v = 1 with more population in v = 1.[9,10,19] Hence the probe was set to detect NO (v = 1, J). The resulting images and translational energy distributions are shown in Figure 5. The inner ring is a background signal arising from NO produced in conjunction with $O(^1D)$ from photodissociation of the NO_2 contaminant by the probe laser alone. The angular distribution for region 2 was found to be similar to that of 2_0^2 for *trans*-HONO in both rotational levels. However, for J = 25.5 region 1 shows slightly higher anisotropy than region 2 (β = −0.81 vs −0.69 for region 2). The anisotropy in region 3 was also slightly higher

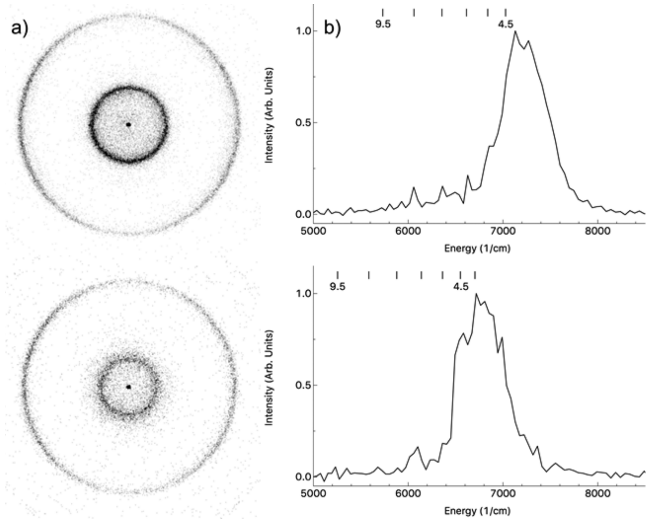

Figure 5. (a) Raw DC sliced images of NO (v''= 1, J'' = 25.5(upper), J'' = 30.5(lower)) rotational levels from photodissociation of *trans*-HONO via 2_0^1 band at 368.30 nm. (b) Corresponding translational energy distribution.

DOI: 10.1021/acs.jpca.7b08120
J. Phys. Chem. A 2017, 121, 7503−7510

compared to the case for the 2_0^2 band. We note in many cases these are small but reproducible trends. From the simulation, we obtain OH(v = 0) rotational temperatures for J = 25.5 and 30.5 rotational levels of 425 and 390 K, respectively.

cis-HONO was also dissociated via the 2_0^1 band. However, at this wavelength, both *cis* and *trans*-HONO have quite similar absorption cross sections. Therefore, the contribution from *trans*-HONO might be significant in these images. The acquired raw images and associated translational energy distributions are shown in Figure 6. In analyzing the images,

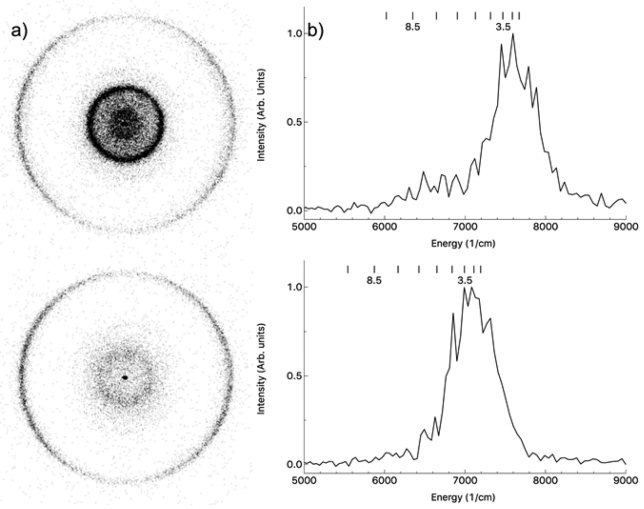

Figure 6. (a) Raw DC sliced images of NO (v = 1, J = 25.5(upper), J = 30.5(lower)) rotational levels from photodissociation of *cis*-HONO via 2_0^1 the band at 364.40 nm. (b) Corresponding translational energy distribution.

an increase of anisotropy in the angular distribution in all the regions and an increase of rotational temperatures is still observed for *cis*- compared to *trans*-HONO. For J'' = 25.5 β changed from −0.69 to −0.83 in region 2, and the rotational temperature of OH cofragment increased from 425 to 440 K. For J'' = 30.5 the anisotropy parameter for region 2 changed from −0.75 to −0.80, and the rotational temperature increased slightly from 390 to 400 K.

DISCUSSION

In 1984, Vasudev, Zare, and Dixon published a detailed investigation of HONO S_1 photodissociation focusing on full characterization of the OH product.[14] They suggested two possible views of the dissociation dynamics: one was predissociation via the ground state as a result of vibronic coupling involving OH torsion, while an alternative was that the dissociation was strictly vibrational predissociation on the diabatic A state.[37] They suggested that in the former case the transition probability should depend on the energy splitting between the ground-state levels involving ν_6 and the prepared S_1 levels containing ν_2 excitation but believed that the incomplete resolution of the spectra precluded confirmation of this mechanism. Their view of the alternative vibrational predissociation mechanism was based on an assumed form of the S_1 potential surface that is flat in the Franck−Condon (FC) region in the NO and ON coordinates, so that the wavepacket is trapped there for some period (50−300 fs) before dissociation along the generally repulsive O−N dimension. That is, there is a "bottleneck" on the surface in the O−N dissociation coordinate. Indeed, there is compelling evidence both in the line widths and in the theoretical dynamics to suggest an increase in lifetime with increasing metastable stretch excitation. All subsequent authors have thus adopted this latter view with some variation, yet there has always been a substantial discrepancy between the short lifetimes based on line width and theory and the longer lifetimes inferred from the angular distributions. We now argue that our results, and much of what is in the literature, are not consistent with a simple picture of parent rotation and lifetime effects responsible for a reduction in the limiting anisotropy. Instead, we associate the nonlimiting anisotropy and the OH rotational excitation to deviation from planarity in the direction of the transition dipole moment associated with OH torsion.

There have long been suggestions of the role of torsion in the extensive literature on this system. By measuring the width of the $\tilde{A}^1A''$−$\tilde{X}^1A'$ transition in a molecular beam at 5 K, Vasudev and co-workers[12] experimentally determined the lifetimes of the $\tilde{A}^1A''$ excited state produced via 2_0^n transitions to be 22 fs for 0° increasing to 96 fs for 2_0^3 excitation. On the basis of the angular distributions and a simple model of the rotation-induced reduction in the anisotropy, Novicki and Vasudev determined fragmentation lifetimes that were significantly longer than would be suggested by the line widths.[10] They assumed the latter were determined by vibrational dephasing, which was described as departure of the wavepacket from the FC region, while the anisotropy was determined by the final fragmentation and associated deviation from axial recoil. Our results, summarized in Table 1, show that even under the conditions of a molecular beam supersonic expansion, we obtain β values very similar to those reported by Vasudev[9,10] and by Dixon and Rieley[19] at room temperature. In 1998 Vasudev and Novicki[9] explored the OH vector correlations and translational energies of vibrational state-selected *trans*-HONO. Although for OH $J \approx 0.5$ the derived value for the anisotropy parameter was at the classical limit, the anisotropy values derived from the bipolar moments for the 0° dissociation showed a deviation from the limiting value for high J OH, and they inferred that the ejected OH experiences an out-of-plane torque. This behavior is just as we see for region 1 in all of our spectra; that is, high rotational levels of OH are indeed associated with reduced anisotropy. Vasudev and Novicki argued there must be a motion along the ν_6 coordinate in the FC region or along the *trans*→*cis* isomerization coordinate. Although there is a barrier for the *trans*→*cis* isomerization in both ground state and excited state and *trans*-HONO is more stable than *cis*-HONO, they suggested that at moderate O−N separations *cis*-HONO might be more stable, even eliminating this barrier. They speculated that as a result OH might experience some out-of-plane kick during the recoil. However, for 2_0^1 and 2_0^2 dissociation the deviation from the limiting value was nevertheless attributed mainly to the parent rotation before fragmentation rather than the out-of-plane impulse.

In 1996 Cotting and Huber[38] reported a comprehensive multireference ab initio study examining many aspects of the excited-state potential-energy surface, including wavepacket dynamics in reduced dimension. In these calculations, the precise character of the FC region was strongly dependent on the level of theory applied, with earlier MCSCF calculations giving a 1500 cm^{-1} deep minimum,[39] while CASPT2 and CASPT2f showed a 50 cm^{-1} for this well, and CISD+Q and

DOI: 10.1021/acs.jpca.7b08120
J. Phys. Chem. A 2017, 121, 7503−7510

CASSCF-f showed no minimum at all. In their three-dimensional (3D) model, they treated OH as a pseudoatom and fixed the scattering angle and the torsional angle at their equilibrium geometries. They examined the dynamics and the absorption spectrum using wavepackets and found lifetimes that were longer for increasing excited-state NO stretch excitation, consistent with experiment, but greater by a factor of 2 or 3. They attempted to include the influence of the bending angle as well, and this reduced the disparity somewhat but did not eliminate it. To explore the role of torsion, they examined one-dimensional (1D) FC factors. They found these to be diagonal for the *trans* form with only small off-diagonal elements for cis. We note that by symmetry, $\nu_6 = 0$ in the ground state can only couple to even levels of ν_6 in S_1. Owing to these small off-diagonal FC factors for torsion, and given the lifetime explanation for the angular distributions, they concluded that torsional excitation does not play a role in the dynamics. However, in addition to calculating the FC factors, they also calculated the torsional vibrational frequencies, and these were found to be dramatically different in S_0 versus S_1: For the *trans* form, ν_6 dropped from 559 cm^{-1} in the ground state to 349 cm^{-1} in S_1, while for the cis form the corresponding change was from 543 to 139 cm^{-1}.

The chief new observation in the present study is in the photofragment angular distributions, which are here obtained under low-temperature conditions and without assumptions regarding the velocity distributions (as was necessary for interpreting the Doppler probe data). Our results show that the deviation from axial recoil owing to parent rotation cannot account for the reduction in anisotropy compared to the perpendicular limit. The anisotropy values we obtain are essentially in quantitative agreement with those obtained by Vasudev and Novicki, including the strongly decreasing anisotropy with OH rotational level. If rotational lifetime effects were solely responsible for the reduction in anisotropy, then our angular distributions would be near the limiting value owing to a 10-fold longer rotational lifetime compared to the room-temperature measurements. Experimental effects that might reduce our measured anisotropy, such as impure polarization, may be safely rejected, as the polarization was controlled with a Berek's compensator and carefully monitored with a Rochon prism. Furthermore, measurements of the anisotropy for S(^{1}D) and CO from OCS photodissociation[35] obtained at the same time gave values in good agreement with the literature.[40]

There are two possible sources for these nonlimiting angular distributions. Either (1) deviation from axial recoil involving out-of-plane motion in the course of dissociation or (2) the transition dipole moment is not strictly perpendicular to the plane of the heavy atoms. We first examine point 1. Deviation from axial recoil may involve either rotational motion of the parent (which we argued may be neglected under the present cold beam conditions given the short lifetime) or a change in the direction of recoil that takes place following photoabsorption but involves internal motions rather than overall rotation of the molecule. This must involve torsional motion of OH, as this is the only motion that can lead the recoil direction out of the initial plane. This torsional displacement, and the associated discrepancy in the angular momentum in the products, give rise to exit orbital angular momentum, which is manifested as rotation of the overall plane in the course of dissociation. We can estimate the maximum effect if we assume the average OH rotational excitation is entirely associated with orbital angular momentum of the system. Taking $L = 5\hbar$ as the average and equating it to the classical expression for the orbital angular momentum, $L = \mu v b$, with μ the reduced mass, v the relative velocity, and b the impact parameter, we obtain an impact parameter of ~10 pm and a deviation of the plane of ~4°. This is consistent with the change in the location of center-of-mass out of the plane associated with large OH torsional displacement. It is not enough to account for the observed effects on the anisotropy, but it may contribute.

The second possibility involves the direction of the transition moment relative to the HO−NO bond that ultimately breaks. Although the transition dipole moment for the planar molecule is indeed strictly perpendicular to this plane, out-of-plane motion of the H atom (ν_6 torsion) leads to a significant deviation of the direction of the transition moment. To investigate the impact of this we performed time-dependent density functional calculations beginning with the ground-state optimized structure, varying only the dihedral angle. We then obtain the angle γ between the transition moment and the breaking N−O bond and determine the associated β parameter using the expression $\beta = 2P_2(\cos\gamma)$, with P_2 the second Legendre polynomial. We choose the N−O bond direction as our reference in defining γ rather that the line joining the centers of mass, as the dissociation shows high rotational excitation in the NO product, and the impulse is largely along that bond direction. The results are shown in Figure 7 for both

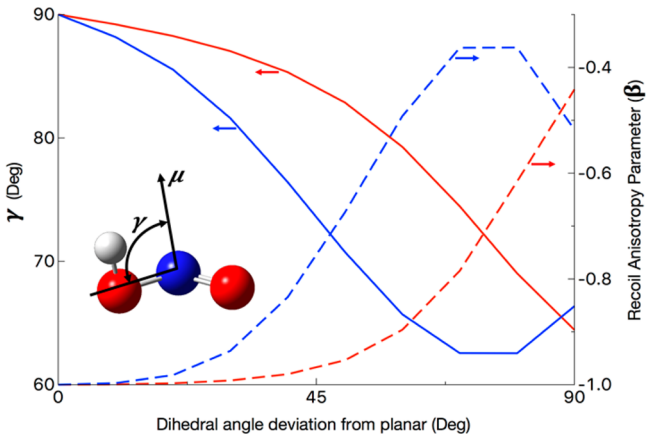

Figure 7. Change in the transition dipole moment (μ) direction (solid) with respect to the N−O bond (γ) of both *cis*-HONO (blue) and *trans*-HONO (red) and corresponding recoil anisotropy parameter (dashed) obtained by time dependent density functional calculation with functional wB97X-D with 6-31G+(d,p) basis set.

trans- and *cis*- conformers. For the *trans* conformer the effect is modest until the dihedral angle is decreased to 100−110°. There we see the transition moment makes an angle of 105−110° with respect to the breaking bond, corresponding to β values in the range of what we observe for the low rotational levels of OH (region 2 in Table 1). Qualitatively, this is precisely the effect we seek to account for the observed angular distributions, although this magnitude of torsional distortion is outside the range of that expected for one quantum in ν_6. For the cis conformer the effect is somewhat larger and becomes significant at much smaller deviation from planar geometry. However, the deviation from perpendicular we see experimentally (Table 1) is actually larger for the trans than the cis, opposite the trend suggested by Figure 7.

DOI: 10.1021/acs.jpca.7b08120
J. Phys. Chem. A 2017, 121, 7503−7510

One other point to note is that dissociation via the origin, although not measured here, was shown to give near-limiting anisotropy. If our interpretation is correct that it is the variation of the transition moment with torsion that affects the angular distributions, this suggests that Franck−Condon mapping onto the vibrational levels of the excited state must significantly impact the direction of the effective transition moment. A dramatic example of this Franck−Condon bias giving rise to strong variation in the transition moment direction and the associated photofragment angular distributions has recently been seen in dissociation of NO-rare gas complexes.[41] We note the result displayed in Figure 7 is a preliminary 1D calculation, and higher-level theory with a full mapping of the transition dipole moment surface is needed to validate this explanation.

These considerations now lead to a discussion of the distinct anisotropy for the different regions of the translational energy release summarized in Table 1. The reduced anisotropy seen for Region 1, associated with rotationally excited OH, has been seen in the past and related to OH torsion. Here we emphasize the correlation between OH rotational excitation and torsional displacement with the direction of the transition dipole moment, to account for this.

We finally turn to consideration of Region 3 of the translational energy distributions, which appears greatest associated with the 2_0^1 excitation. It is possible this represents hot-band contributions involving one quanta of v_6, the lowest-frequency vibrational level in the ground state. At room temperature, we would predict the population of this mode to be ∼7%. For this to overlap the 2_0^1 band it would have to involve a combination in S_1, but this is certainly possible. This would lead to a corresponding shift of the translational energy release just as we see. We see an offset of 300−400 cm^{-1}, but this could be compensated by greater OH rotational excitation in this case. Indeed, the greatly reduced anisotropy in region 3 is consistent with our picture of the role of OH torsion. The other point to recognize is that the higher OH rotational levels from a hot band contribution could partly overlap the main peak and perhaps contribute to the reduced anisotropy there. At this point we can only offer speculation, and a definitive explanation must await future investigations.

In summary, we have presented the first imaging study of HONO photodissociation. Both *trans*- and *cis*-HONO were photodissociated via 2_0^2 band and 2_0^1 of the $\tilde{A}^1A''-\tilde{X}^1A'$ transition. The observed recoil anisotropy parameters in both bands were between −0.6 and −0.8. We ascribe this deviation from the limiting value to change in the direction of the transition dipole moment with respect to the plane of the heavy atoms associated with the torsional coordinate, rather than deviation from axial recoil induced by parent rotation as in earlier work. In both bands, *cis*-HONO was slightly more anisotropic than the *trans*-HONO, and this observation was attributed to the intramolecular hydrogen bonding present in the *cis*-HONO. An additional feature in the translation energy release showing greatly reduced anisotropy is ascribed to hot band excitation involving v_6.

AUTHOR INFORMATION

Corresponding Author

*E-mail: suitsa@missouri.edu.

ORCID

Arthur G. Suits: 0000-0001-5405-8361

Notes

The authors declare no competing financial interest.

ACKNOWLEDGMENTS

The authors would like to acknowledge G. Hall and R. W. Field for helpful discussions. This work was supported by the Army Research Office under Award No. W911NF-14-1-0378.

REFERENCES

(1) Emmerson, K. M.; Carslaw, N. Night-time radical chemistry during the TORCH campaign. *Atmos. Environ.* **2009**, *43* (20), 3220−3226.

(2) Stone, D.; Whalley, L. K.; Heard, D. E. Tropospheric OH and HO2 radicals: field measurements and model comparisons. *Chem. Soc. Rev.* **2012**, *41* (19), 6348−6404.

(3) Perner, D.; Platt, U. Detection of nitrous acid in the atmosphere by differential optical absorption. *Geophys. Res. Lett.* **1979**, *6* (12), 917−920.

(4) Spataro, F.; Ianniello, A. Sources of atmospheric nitrous acid: State of the science, current research needs, and future prospects. *J. Air Waste Manage. Assoc.* **2014**, *64* (11), 1232−1250.

(5) VandenBoer, T. C.; Young, C. J.; Talukdar, R. K.; Markovic, M. Z.; Brown, S. S.; Roberts, J. M.; Murphy, J. G. Nocturnal loss and daytime source of nitrous acid through reactive uptake and displacement. *Nat. Geosci.* **2014**, *8* (1), 55−60.

(6) Lammel, G.; Cape, J. N. Nitrous acid and nitrite in the atmosphere. *Chem. Soc. Rev.* **1996**, *25* (5), 361−369.

(7) Indarto, A. Heterogeneous reactions of HONO formation from NO2 and HNO3: a review. *Res. Chem. Intermed.* **2012**, *38* (3), 1029−1041.

(8) Ren, X.; Harder, H.; Martinez, M.; Lesher, R. L.; Oliger, A.; Simpas, J. B.; Brune, W. H.; Schwab, J. J.; Demerjian, K. L.; He, Y.; Zhou, X.; Gao, H. OH and HO2 Chemistry in the urban atmosphere of New York City. *Atmos. Environ.* **2003**, *37* (26), 3639−3651.

(9) Vasudev, R.; Novicki, S. W. SubDoppler polarization spectroscopy of OH ejected by vibrational state-selected trans HONO(Ã 1A″): OH vector correlations, energy correlation between coincident OH,NO pairs, and energy transfer pathways. *Chem. Phys.* **1998**, *226* (1−2), 201−215.

(10) Novicki, S. W.; Vasudev, R. Doppler spectroscopy of the OH fragment ejected by trans HONO (Ã 1A′): Characterization of the Ã state resonances and determination of vibrational energy content of the NO fragment. *J. Chem. Phys.* **1991**, *95* (10), 7269−7274.

(11) Shan, J. H.; Wategaonkar, S. J.; Vasudev, R. State-selected dissociation of cis-HONO(Ã 1A″): Effect of intramolecular hydrogen bonding. *Chem. Phys. Lett.* **1989**, *160* (5), 614−617.

(12) Shan, J. H.; Wategaonkar, S. J.; Vasudev, R. Vibrational state dependence of the Ã, state lifetime of HONO. *Chem. Phys. Lett.* **1989**, *158* (3), 317−320.

(13) Shan, J. H.; Vasudev, R. Effect of intramolecular dynamics on state-to-state photochemistry: Fragmentation of the Ã state of trans-DONO. *Chem. Phys. Lett.* **1987**, *141* (6), 472−477.

(14) Vasudev, R.; Zare, R. N.; Dixon, R. N. State-selected photodissociation dynamics: Complete characterization of the OH fragment ejected by the HONO Ã state. *J. Chem. Phys.* **1984**, *80* (10), 4863−4878.

(15) Vasudev, R.; Zare, R. N.; Dixon, R. N. Dynamics of photodissociation of hono at 369 nm: Motional anisotropy and internal state distribution of the OH fragment. *Chem. Phys. Lett.* **1983**, *96* (4), 399−402.

(16) King, G. W.; Moule, D. The ultraviolet absorption spectrum of nitrous acid in the vapoer state. *Can. J. Chem.* **1962**, *40* (11), 2057−2065.

(17) Bongartz, A.; Kames, J.; Welter, F.; Schurath, U. Near-UV absorption cross sections and trans/cis equilibrium of nitrous acid. *J. Phys. Chem.* **1991**, *95* (3), 1076−1082.

(18) Reiche, F.; Abel, B.; Beck, R. D.; Rizzo, T. R. Double-resonance overtone photofragment spectroscopy of trans-HONO. I. Spectrosco-

DOI: 10.1021/acs.jpca.7b08120
J. Phys. Chem. A 2017, 121, 7503−7510

py and intramolecular dynamics. *J. Chem. Phys.* **2000**, *112* (20), 8885−8898.
(19) Dixon, R. N.; Rieley, H. State-selected photodissociation dynamics of HONO(Ã 1A′): Characterization of the NO fragment. *J. Chem. Phys.* **1989**, *91* (4), 2308−2320.
(20) Jones, L. H.; Badger, R. M.; Moore, G. E. The Infrared Spectrum and the Structure of Gaseous Nitrous Acid. *J. Chem. Phys.* **1951**, *19* (12), 1599−1604.
(21) McGraw, G. E.; Bernitt, D. L.; Hisatsune, I. C. Infrared Spectra of Isotopic Nitrous Acids. *J. Chem. Phys.* **1966**, *45* (5), 1392−1399.
(22) Varma, R.; Curl, R. F. Study of the dinitrogen trioxide-water-nitrous acid equilibrium by intensity measurements in microwave spectroscopy. *J. Phys. Chem.* **1976**, *80* (4), 402−409.
(23) Turner, A. G. An ab initio study of isomerization in the nitrous acid (HONO) system. *J. Phys. Chem.* **1985**, *89* (21), 4480−4483.
(24) Richter, F.; Hochlaf, M.; Rosmus, P.; Gatti, F.; Meyer, H.-D. A study of the mode-selective trans−cis isomerization in HONO using ab initio methodology. *J. Chem. Phys.* **2004**, *120* (3), 1306−1317.
(25) Sironneau, V.; Flaud, J. M.; Orphal, J.; Kleiner, I.; Chelin, P. Absolute line intensities of HONO and DONO in the far-infrared and re-determination of the energy difference between the trans- and cis-species of nitrous acid. *J. Mol. Spectrosc.* **2010**, *259* (2), 100−104.
(26) Pradhan, E.; Brown, A. A ground state potential energy surface for HONO based on a neural network with exponential fitting functions. *Phys. Chem. Chem. Phys.* **2017**, *19* (33), 22272−22281.
(27) Finnigan, D. J.; Cox, A. P.; Brittain, A. H.; Smith, J. G. Centrifugal distortion in the microwave spectra of cis- and trans-nitrous acids. Determination of the quadratic potential functions and average structures. *J. Chem. Soc., Faraday Trans. 2* **1972**, *68* (0), 548−565.
(28) Murto, J.; Räsänen, M.; Aspiala, A.; Lotta, T. Ab initio calculations on hono: Energies, geometries and force fields on different levels of theory. *J. Mol. Struct.: THEOCHEM* **1985**, *122* (3), 213−224.
(29) Guan, Y.; Lynch, G. C.; Thompson, D. L. Intramolecular energy transfer and cis−trans isomerization in HONO. *J. Chem. Phys.* **1987**, *87* (12), 6957−6966.
(30) Chandler, D. W.; Houston, P. L. Two-dimensional imaging of state-selected photodissociation products detected by multiphoton ionization. *J. Chem. Phys.* **1987**, *87* (2), 1445−1447.
(31) Eppink, A. T. J. B.; Parker, D. H. Velocity map imaging of ions and electrons using electrostatic lenses: Application in photoelectron and photofragment ion imaging of molecular oxygen. *Rev. Sci. Instrum.* **1997**, *68* (9), 3477−3484.
(32) Townsend, D.; Minitti, M. P.; Suits, A. G. Direct current slice imaging. *Rev. Sci. Instrum.* **2003**, *74* (4), 2530−2539.
(33) Luque, J.; Crosley, D. *Lifbase: Database and Spectral Simulation Program,* version 1.5; SRI International Report MP 99-009, 1999.
(34) Stutz, J.; Kim, E. S.; Platt, U.; Bruno, P.; Perrino, C.; Febo, A. UV-visible absorption cross sections of nitrous acid. *J. Geophys. Res.* **2000**, *105*, 14585.
(35) Thompson, J. O. F.; Amarasinghe, C.; Foley, C. D.; Suits, A. G. Finite slice analysis (FINA)—A general reconstruction method for velocity mapped and time-sliced ion imaging. *J. Chem. Phys.* **2017**, *147* (1), 013913.
(36) Thompson, J. O. F.; Amarasinghe, C.; Foley, C. D.; Rombes, N.; Gao, Z.; Vogels, S. N.; van de Meerakker, S. Y. T.; Suits, A. G. Finite slice analysis (FINA) of sliced and velocity mapped images on a Cartesian grid. *J. Chem. Phys.* **2017**, *147* (7), 074201.
(37) Herzberg, G. *Molecular Spectra and Molecular Structure;* Van Nostrand: New York, 1966; Vol. *III*.
(38) Cotting, R.; Huber, J. R. Predissociation of HONO upon excitation into the S1 state: An ab initio and dynamics study. *J. Chem. Phys.* **1996**, *104* (16), 6208−6224.
(39) Hennig, S.; Untch, A.; Schinke, R.; Nonella, M.; Huber, J. R. Theoretical investigation of the photodissociation dynamics of HONO: Vibrational predissociation in the electronically excited state S1. *Chem. Phys.* **1989**, *129* (1), 93−107.
(40) Weeraratna, C.; Amarasinghe, C.; Fernando, R.; Tiwari, V.; Suits, A. G. Convenient (1 + 1) probe of S(1D2) and application to photodissociation of carbonyl sulfide at 216.9 nm. *Chem. Phys. Lett.* **2016**, *657*, 162−166.
(41) Holmes-Ross, H. L.; Valenti, R. J.; Yu, H.-G.; Hall, G. E.; Lawrance, W. D. Rotational and angular distributions of NO products from NO-Rg (Rg = He, Ne, Ar) complex photodissociation. *J. Chem. Phys.* **2016**, *144* (4), 044309.

DOI: 10.1021/acs.jpca.7b08120
J. Phys. Chem. A 2017, 121, 7503−7510